Rayleigh-like distribution of particle transverse momenta in collisions at high energies*

SHAO Gui-Cheng(邵贵成)[1,1)] LI Hui-Ling(李惠玲)[2]

[1] Department of Physics, Xinzhou Normal University, Xinzhou 034000, China
[2] Department of Physics, Shanxi Normal University, Linfen 041004, China

Abstract The transverse momentum distributions of final-state particles produced in collisions at high energies are studied by using a two-component Rayleigh-like distribution. This representation is based on Liu's multisource ideal gas model which describes protons and fragments in high energy nucleus-nucleus collisions. The calculated results are in good agreement with the experimental data of Au-Au, Cu-Cu, d-Au, and pp collisions at the relativistic heavy ion collider energies. The experimental particle momentum distributions of p-Be collisions at 6.4, 12.3, and 17.5 GeV/c, as well as Au-Au collisions at 1.5 AGeV are well described by a model based on a single Rayleigh-like distribution of particle transverse momenta.

Key words transverse momentum distribution, Rayleigh-like distribution, high energy collisions

PACS 24.10.Pa, 25.40.Ve, 13.85.Ni

1 Introduction

In high energy collisions [1–4], the measured particle distributions [5–9] retain information about the production process and allow the degree of source excitation to be determined [10]. To explain the abundant experimental data [11–14], different phenomenological mechanisms of initial coherent multiple interactions and particle transports were proposed [15–18]. In a recent workshop [19] held at the CERN Theory Institute, many models have reported their last results.

The transverse momentum (transverse mass) distributions of identified hadrons produced in Au-Au collisions at the relativistic heavy ion collider (RHIC) and alternating gradient synchrotron (AGS) energies have been discussed in one of Liu's recent works [20]. It is shown in that reference that a single component distribution describes well the experimental data. However, Liu has shown in another work [21] that the transverse momentum distributions of identified hadrons produced in Cu-Cu, d-Au, and pp collisions at RHIC energy cannot be described by a single component distribution and that a two-component distribution has to be considered in the description of transverse momentum distributions.

In this article in order to give a further investigation on the transverse momentum distributions, we propose another formula, namely the (two-component) Rayleigh-like distribution, to describe the experimental transverse momentum distributions. The second section describes the model. The third section shows comparisons between the calculated results and experimental data. Finally, conclusions and discussions are given in the last section.

2 The model

For comparison with the present model, we introduce shortly the two-component semi-empirical formula introduced in Ref. [21]. In the framework of the thermalized cylinder picture, according to the single component distribution [20], the transverse momentum distribution of final-state particles is described by

$$f_{1p_{\rm T}}(p_{\rm T},\sigma_{\rm c},\sigma_{\rm s})=C\int_{\sigma_{\rm s}}^{\sigma_{\rm c}}(\sigma_{\rm c}-\sigma)\frac{p_{\rm T}}{\sigma^2}\exp\left(-\frac{p_{\rm T}^2}{2\sigma^2}\right)\mathrm{d}\sigma, \quad (1)$$

where $\sigma_{\rm c}$ and $\sigma_{\rm s}$ denote the momentum distribution widths of particles produced in the central axis and

Received 22 September 2009
* Supported by NSFC (10675077, 10975095) and Natural Science Foundation of Shanxi Province (2007011005)
1) E-mail: guichengshao@163.com

side-surface regions respectively, σ is an integral variable denoting the momentum distribution width of particles produced in a given region of the cylinder, and C is the normalization constant. The value of C depends on the choice of $\sigma_{\rm c}$ and $\sigma_{\rm s}$.

For the two-component distribution, we have

$$f_1(p_{\rm T}) = kf_{1p_{\rm T}}(p_{\rm T},\sigma_{1\rm c},\sigma_{1\rm s}) + (1-k)f_{1p_{\rm T}}(p_{\rm T},\sigma_{2\rm c},\sigma_{2\rm s}), \quad (2)$$

where $k(1-k)$ gives the relative contribution of the first (second) term, $\sigma_{1\rm c}$ ($\sigma_{2\rm c}$) and $\sigma_{1\rm s}$ ($\sigma_{2\rm s}$) are the momentum distribution widths of particles produced in the central axis and side-surface regions of the first (second) term respectively. In Eq. (2), there are five free parameters k, $\sigma_{1\rm c}$, $\sigma_{1\rm s}$, $\sigma_{2\rm c}$, and $\sigma_{2\rm s}$. Generally speaking, we choose $\sigma_{1\rm c} \leqslant \sigma_{2\rm c}$ and $\sigma_{1\rm s} \leqslant \sigma_{2\rm s}$. The contribution of the first term in Eq. (2) covers the region from low to high $p_{\rm T}$ and the second term in Eq. (2) dominates at higher $p_{\rm T}$.

The present model is a revised and extended version of Liu's multisource ideal gas model [22, 23] which describes well protons and fragments emitted in high energy collisions. According to Liu's multisource ideal gas model, many emission sources are assumed to form in the collisions. In the rest frame of a considered source, we assume that the particles and fragments are isotropically emitted, and the momentum components have a Gaussian distribution with the same width. The interactions among different emission sources will cause the emission sources to have different expansions and displacements [22, 23]. As a result, the measured momentum components p_x and p_y of the final-state products have different distribution widths and mean values. This means that the transverse momentum $\boldsymbol{p_T} = p_x\boldsymbol{i}+p_y\boldsymbol{j}$ in Liu's multisource ideal gas model is not a real Rayleigh distribution, but a Rayleigh-like distribution. Because of the anisotropic p_x and p_y distributions, elliptic (v_2) and directed (v_1) flows are observed in experiments.

Considering the interactions among different emission sources [22, 23], p_x and p_y can be assumed to obey Gaussian distributions having different widths (σ_x and σ_y) and different mean values ($\langle p_x\rangle$ and $\langle p_y\rangle$). Generally speaking, we can choose a satisfactory coordinate system and have $\langle p_x\rangle = \langle p_y\rangle = 0$. According to probability theory, the single component distribution of particle transverse momenta is given by

$$f_{2p_{\rm T}}(p_{\rm T},\sigma_x,\sigma_y) = \frac{p_{\rm T}}{2\pi\sigma_x\sigma_y} \times \int_0^{2\pi} \exp\left[-\frac{p_{\rm T}^2}{2}\left(\frac{\cos^2\varphi}{\sigma_x^2}+\frac{\sin^2\varphi}{\sigma_y^2}\right)\right]{\rm d}\varphi, \quad (3)$$

where φ is an integration variable denoting the azimuthal angle of the final-state particle. In the case of the xoz plane being the reaction plane, we have $\sigma_x \geqslant \sigma_y$. Eq. (3) can be called a Rayleigh-like distribution. Especially, Eq. (3) will be a Rayleigh distribution, i.e. $f_{2p_{\rm T}} = (p_{\rm T}/\sigma^2)\exp(-p_{\rm T}^2/2\sigma^2)$, in the case of $\sigma_x = \sigma_y = \sigma$.

The two-component Rayleigh-like distribution can be given by

$$f_2(p_{\rm T}) = Kf_{2p_{\rm T}}(p_{\rm T},\sigma_{1x},\sigma_{1y}) + (1-K)f_{2p_{\rm T}}(p_{\rm T},\sigma_{2x},\sigma_{2y}), \quad (4)$$

where $K(1-K)$ and $\sigma_{1x,1y}$ ($\sigma_{2x,2y}$) gives the relative contribution and distribution widths of the first (second) term respectively. In Eq. (4), there are also five free parameters K, σ_{1x}, σ_{1y}, σ_{2x}, and σ_{2y}. Generally speaking, we choose $\sigma_{1x} \leqslant \sigma_{2x}$ and $\sigma_{1y} \leqslant \sigma_{2y}$. As in Eq. (2), the contribution of the first term in Eq. (4) covers the region from low to high $p_{\rm T}$ and the second term dominates at higher $p_{\rm T}$.

As a natural extension of Maxwell's ideal gas model, the Rayleigh distribution is a special Rayleigh-like distribution in the case of $\sigma_x = \sigma_y = \sigma$. For a given event sample, the parameter K denotes the fraction of particles described by the first term in Eq. (4). Naturally, the fraction of particles described by the second term is $1-K$. The parameters σ_{1x} and σ_{1y} denote respectively the distribution widths of p_x and p_y of the particles described by the first term; and the parameters σ_{2x} and σ_{2y} denote respectively those of the particles described by the second term.

To describe easily the momentum distributions, we may also use the Monte Carlo method. Considering the expressions for random variables with Gaussian distributions, we have

$$p_{x,y} = \sigma_{x,y}\sqrt{-2\ln R_{1,3}}\cos(2\pi R_{2,4}) + \langle p_{x,y}\rangle, \quad (5)$$

where R_1, R_2, R_3, and R_4 denote random numbers in $[0,1]$. $p_{\rm T}$ is given by

$$p_{\rm T} = \left\{\left[\sigma_x\sqrt{-2\ln R_1}\cos(2\pi R_2)+\langle p_x\rangle\right]^2 + \left[\sigma_y\sqrt{-2\ln R_3}\cos(2\pi R_4)+\langle p_y\rangle\right]^2\right\}^{1/2}. \quad (6)$$

The total momentum of the particle is related to $p_{\rm T}$ by the relation $p = p_{\rm T}/\sin\vartheta$, where ϑ is the emission polar angle. In the case of $\sigma_x = \sigma_y = \sigma$ and $\langle p_x\rangle = \langle p_y\rangle = 0$, one obtains that $p_{\rm T}$ has a Rayleigh distribution, i.e. $p_{\rm T} = \sigma\sqrt{-2\ln R_5}$, where R_5 denotes random numbers in $[0,1]$.

In the above discussions the distribution width σ_y ($\sigma_{1y,2y}$) is related to the degree of excitation of

the emission sources, and the ratio $\sigma_x/\sigma_y \geqslant 1$ denotes the strength of the interactions among different emission sources or the expansion coefficient of the emission source along the ox axis. In the framework of Maxwell's ideal gas model we have $\sigma_y = \sqrt{mT}$, where m and T denote the mass of the considered particle and the temperature of the emission source respectively. It is expected that the temperature of the emission source, and then with it the distribution width of particle momenta increases with increasing incident (center-of-mass) energy and the system size if other factors are fixed. The distribution width of the particle momenta increases also with the particle mass for a given interaction system. It is observed that the fraction K of the first term decreases with increasing center-of-mass energy.

3 Comparison with experimental data

The transverse momentum distributions of ϕ particles, $(1/2\pi p_{\rm T})\mathrm{d}^2N/\mathrm{d}p_{\rm T}\mathrm{d}y$, produced in Au-Au collisions at a nucleon-nucleon center-of-mass energy of $\sqrt{s_{\rm NN}} = 200$ GeV is presented in Fig. 1. The circles and squares represent the experimental data of the STAR Collaboration [24] for different centrality cuts as marked in the figure. The dotted and dashed curves are our results calculated using Eqs. (2) and (4) respectively. The values of k, $\sigma_{1\rm c}$, $\sigma_{1\rm s}$, $\sigma_{2\rm c}$, and $\sigma_{2\rm s}$ obtained by fitting the experimental data are given in Table 1 with the resulting χ^2 per degree of freedom (dof). The values of K, σ_{1x}, σ_{1y}, σ_{2x}, and σ_{2y} obtained by fitting the experimental data are given in Table 2. In the tables, the values of $\sigma_{1\rm c}$ and $\sigma_{1\rm s}$ ($\sigma_{2\rm c}$ and $\sigma_{2\rm s}$) are given in terms of $\sigma_{1\rm c}$-$\sigma_{1\rm s}$ ($\sigma_{2\rm c}$-$\sigma_{2\rm s}$), and the values of σ_{1x} and σ_{1y} (σ_{2x} and σ_{2y}) are given in terms of σ_{1x}-σ_{1y} (σ_{2x}-σ_{2y}). One can see that not only Eq. (2) but also Eq. (4) describe well the $p_{\rm T}$ distributions of the ϕ particles produced in Au-Au collisions at the maximum RHIC energy.

Similar results for the reaction Cu-Cu at $\sqrt{s_{\rm NN}} =$ 22.5 GeV are shown in Fig. 2. The symbols represent the experimental data of the PHENIX Collaboration [25] for different centrality cuts as marked in the figure. The J/ψ invariant yield versus $p_{\rm T}$ in d-Au collisions at $\sqrt{s_{\rm NN}} = 200$ GeV are given in Fig. 3. The results are shown for three rapidity ranges with different Global Scale Uncertainties (GSUs). The circles and squares represent the experimental data of the PHENIX Collaboration [26]. Fig. 4 presents the transverse momentum distributions, $(1/2\pi p_{\rm T})B\mathrm{d}^2\sigma/\mathrm{d}p_{\rm T}\mathrm{d}y$, of J/ψ particles produced in pp collisions at $\sqrt{s_{\rm NN}} = 200$ GeV, where σ and B denote the cross section and the di-lepton branching ratio respectively. The results are shown for two rapidity ranges with different GSUs. The circles and squares represent the experimental data of the PHENIX Collaboration [27, 28]. In Figs. 2–4 the dotted curves are Liu's previous results [21] calculated

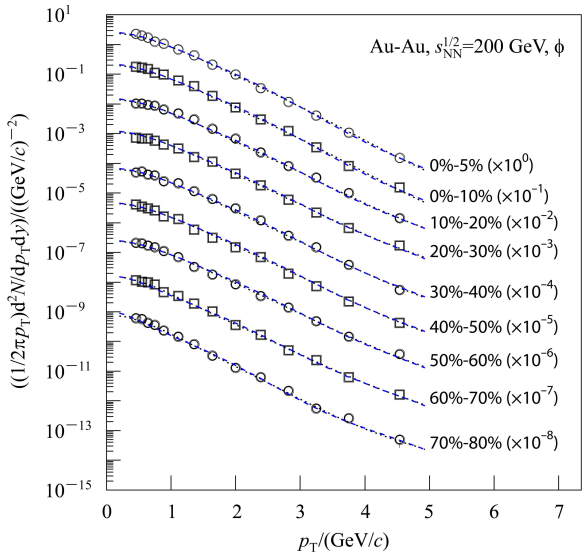

Fig. 1. Transverse momentum distributions of ϕ produced in Au-Au collisions at $\sqrt{s_{\rm NN}} = 200$ GeV. The circles and squares represent the experimental data of the STAR Collaboration [24]. The dotted and dashed curves are our calculated results by Eqs. (2) and (4) respectively.

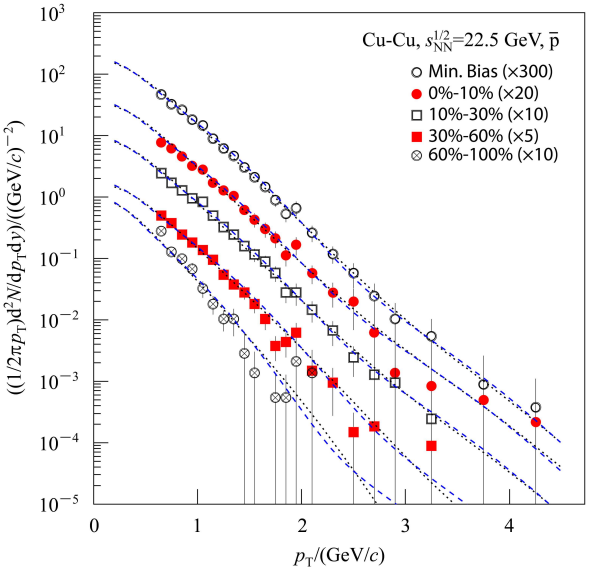

Fig. 2. Transverse momentum distributions of p̄ produced in Cu-Cu collisions at $\sqrt{s_{\rm NN}} =$ 22.5 GeV. The symbols represent the experimental data of the PHENIX Collaboration [25]. The dotted and dashed curves are Liu's previous [21] and our present results calculated by Eqs. (2) and (4) respectively.

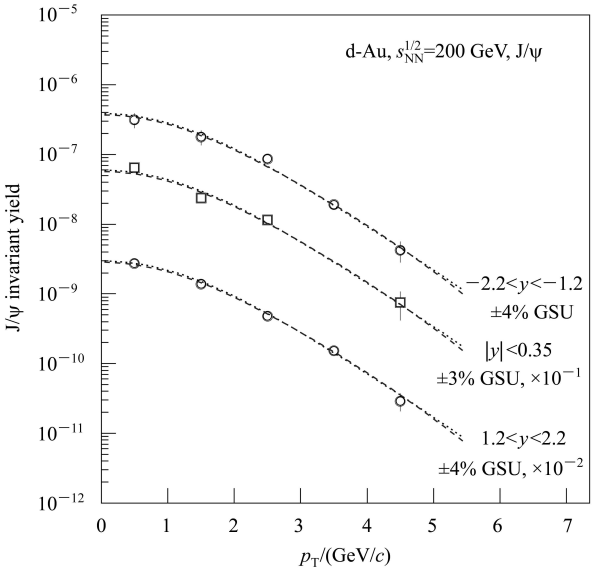

Fig. 3. J/ψ invariant yield versus transverse momentum in d-Au collisions at $\sqrt{s_{NN}} = 200$ GeV. The circles and squares represent the experimental data of the PHENIX Collaboration [26]. The dotted and dashed curves are Liu's previous [21] and our present results, calculated with Eqs. (2) and (4) respectively.

using Eq. (2), and the dashed curves are our results calculated using Eq. (4). The parameter values obtained by fitting the experimental data are given in Tables 1 and 2. The comparisons show that Eq. (4) gives a good description of the p_T data.

The momentum distributions, $d^2\sigma/dpd\Omega$, of π^+ and π^- mesons produced in p-Be collisions at 6.4, 12.3, and 17.5 GeV/c are shown in Fig. 5. The circles and squares represent the experimental data of Chemakin et al. [29] for different emission angles, scaled by the amount indicated in the legend. The curves are our calculated results using Eq. (6). The values of σ_x and σ_y are given in Table 3. In the fitting for π^+ at $\vartheta = 71$ mrad, we have $\langle p_x\rangle = 0.02$ GeV/c and $\langle p_y\rangle = 0.05$ GeV/c. In the fitting for π^- assuming $\vartheta = 353$ mrad, we have $\langle p_x\rangle = 0.08$ GeV/c and $\langle p_y\rangle = 0.05$ GeV/c. In other fittings, we have $\langle p_x\rangle = \langle p_y\rangle = 0$. One can see that the model describes well the experimental data of p-Be collisions.

The momentum distributions, $d\sigma/dpd\Omega$, of π^- mesons produced in Au-Au collisions at 1.5 AGeV are presented in Fig. 6. The symbols represent the experimental data of the FOPI and KaoS Collaborations [30] for two emission angles, scaled by the amount indicated in the legend. The curves are our calculated results. In the fitting for $\vartheta = 40°$, we have $\sigma_x = 0.184$ GeV/c, $\sigma_y = 0.038$ GeV/c, $\langle p_x\rangle = 0.070$ GeV/c, and $\langle p_y\rangle = 0.080$ GeV/c with χ^2/dof=0.12. In the fitting assuming $\vartheta = 60°$, we have $\sigma_x = 0.195$ GeV/c, $\sigma_y = 0.041$ GeV/c, $\langle p_x\rangle = 0.078$ GeV/c, and $\langle p_y\rangle = 0.086$ GeV/c with χ^2/dof=0.13. One can see that our simple model describes very well the experimental data of Au-Au collisions at 1.5 AGeV.

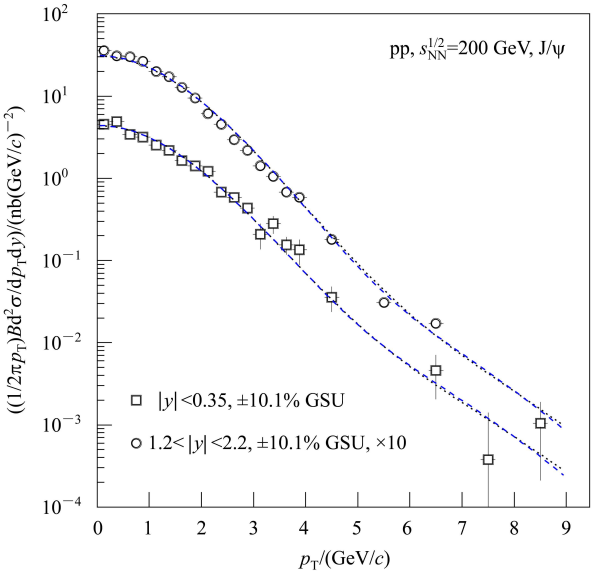

Fig. 4. J/ψ differential cross section times dilepton branching ratio versus transverse momentum in pp collisions at $\sqrt{s_{NN}} = 200$ GeV. The circles represent the experimental data of the PHENIX Collaboration [27, 28]. The dotted and dashed curves are Liu's previous [21] and our present results, calculated with Eqs. (2) and (4) respectively.

4 Conclusions and discussions

To conclude, the p_T distributions of final-state particles produced in Au-Au, Cu-Cu, d-Au, and pp collisions at the RHIC energies are studied using a two-component Rayleigh-like distribution. This representation with a single component distribution is a natural extension of Liu's multisource ideal gas model, and the two-component distribution is obtained by a semi-empirical consideration. It is shown that the model is successful in the description of p_T distributions of final-state particles produced in high energy collisions. From Table 2 we see that the distribution width (Figs. 3 and 4) has a relatively large value in the large interaction system.

As in Eq. (2), the contribution of the second term in Eq. (4) is very small; in some cases, the second term contributes zero (Fig. 3). The distribution width of the first term does not show a change in central and semi-central collisions, and the concerned quantity has a small decrease in peripheral collisions. The dis-

tribution width of the second term does not show a change with decreasing centrality (Fig. 1) or has a small change in peripheral collisions (Fig. 2).

A single Rayleigh-like distribution is used to give a description of the particle transverse momenta in fixed target experiments. The momentum distribution of particles with a given emission angle is easily obtained. The calculated results of the particle momentum distributions are compared and found to be in good agreement with the experimental data of p-Be and Au-Au collisions at the low-end of high energies. From Table 3 we see that the mean value of the distribution widths increases slightly with the incident energy in the considered energy range.

Table 1. Values of the parameters k, σ_{1c}-σ_{1s}, and σ_{2c}-σ_{2s} for the dotted curves in Figs. 1–4. The units of σ_{1c}, σ_{1s}, σ_{2c}, and σ_{2s} are GeV/c.

figure	cut condition	k(%)	σ_{1c}-σ_{1s}	σ_{2c}-σ_{2s}	χ^2/dof
Fig. 1	0%–5%	99.90	1.40–0.50	2.40–1.60	0.45
	0%–10%	99.90	1.40–0.50	2.40–1.60	0.79
	10%–20%	99.70	1.40–0.50	2.40–1.60	1.07
	20%–30%	99.60	1.40–0.50	2.40–1.60	0.33
	30%–40%	99.70	1.40–0.50	2.40–1.60	0.74
	40%–50%	99.70	1.40–0.50	2.40–1.60	0.32
	50%–60%	99.60	1.40–0.50	2.40–1.60	0.55
	60%–70%	99.60	1.40–0.40	2.40–1.60	0.58
	70%–80%	99.70	1.30–0.40	2.40–1.60	0.94
Fig. 2*	Min. Bias	99.70	0.90–0.30	1.30–1.08	0.62
	0%–10%	99.40	0.90–0.30	1.30–1.08	1.14
	10%–30%	99.50	0.90–0.30	1.30–1.08	0.68
	30%–60%	99.90	0.90–0.30	1.30–1.08	1.33
	60%–100%	100.00	0.78–0.25	–	1.35
Fig. 3*	$-2.2 < y < -1.2$	100.00	2.40–1.00	–	0.23
	$\|y\| < 0.35$	100.00	2.40–1.00	–	0.82
	$1.2 < y < 2.2$	100.00	2.40–1.00	–	0.24
Fig. 4*	$1.2 < \|y\| < 2.2$	99.00	2.00–1.00	3.60–2.40	0.67
	$\|y\| < 0.35$	98.00	2.00–1.00	3.60–2.40	0.80

∗ The parameter values and corresponding dotted curves are taken from Ref. [21] for comparison.

Table 2. Values of the parameters K, σ_{1x}-σ_{1y}, and σ_{2x}-σ_{2y} for the dashed curves in Figs. 1–4. The units of σ_{1x}, σ_{1y}, σ_{2x}, and σ_{2y} are GeV/c.

figure	cut condition	K(%)	σ_{1x}-σ_{1y}	σ_{2x}-σ_{2y}	χ^2/dof
Fig. 1	0%–5%	98.80	1.06–0.47	1.90–1.40	0.46
	0%–10%	98.80	1.06–0.47	1.90–1.40	0.71
	10%–20%	98.00	1.06–0.47	1.90–1.40	1.00
	20%–30%	97.60	1.06–0.47	1.90–1.40	0.36
	30%–40%	97.80	1.06–0.47	1.90–1.40	0.55
	40%–50%	97.80	1.06–0.47	1.90–1.40	0.38
	50%–60%	97.60	1.06–0.47	1.90–1.40	0.65
	60%–70%	97.20	1.03–0.35	1.90–1.40	0.94
	70%–80%	98.00	0.96–0.30	1.90–1.40	1.18
Fig. 2	Min. Bias	98.92	0.69–0.26	1.47–0.86	0.41
	0%–10%	98.15	0.69–0.26	1.47–0.86	1.11
	10%–30%	98.60	0.69–0.26	1.47–0.86	0.39
	30%–60%	99.40	0.69–0.26	1.47–0.86	0.87
	60%–100%	99.60	0.58–0.22	1.20–0.90	1.62
Fig. 3	$-2.2 < y < -1.2$	100.00	1.88–1.00	–	0.22
	$\|y\| < 0.35$	100.00	1.88–1.00	–	0.82
	$1.2 < y < 2.2$	100.00	1.88–1.00	–	0.24
Fig. 4	$1.2 < \|y\| < 2.2$	97.30	1.60–1.00	3.00–2.50	0.63
	$\|y\| < 0.35$	94.80	1.60–1.00	3.00–2.50	0.88

Table 3. Values of the parameters σ_x and σ_y for the curves in Fig. 5.

type	ϑ/mrad	$\sigma_x/(\mathrm{GeV}/c)$	$\sigma_y/(\mathrm{GeV}/c)$	χ^2/dof	v_2 ($>$ or $=0$)
6.4 GeV/c, π^+	71	0.10	0.08	0.21	>0
	158	0.16	0.16	0.87	$=0$
	255	0.21	0.21	0.83	$=0$
	353	0.40	0.15	1.22	>0
6.4 GeV/c, π^-	71	0.12	0.05	0.39	>0
	158	0.25	0.06	1.21	>0
	255	0.35	0.10	1.33	>0
	353	0.34	0.12	0.86	>0
12.3 GeV/c, π^+	42	0.09	0.09	0.14	$=0$
	95	0.23	0.12	0.21	>0
	153	0.31	0.12	0.27	>0
	212	0.33	0.12	1.04	>0
	272	0.33	0.14	1.40	>0
	331	0.37	0.14	0.64	>0
12.3 GeV/c, π^-	42	0.12	0.05	0.38	>0
	95	0.20	0.11	0.35	>0
	153	0.26	0.14	1.50	>0
	212	0.27	0.14	0.83	>0
	272	0.37	0.13	0.60	>0
	331	0.33	0.14	0.54	>0
17.5 GeV/c, π^+	42	0.11	0.11	0.28	$=0$
	95	0.26	0.12	0.16	>0
	153	0.34	0.14	0.22	>0
	212	0.37	0.13	0.43	>0
	272	0.35	0.14	1.17	>0
	331	0.35	0.16	0.66	>0
17.5 GeV/c, π^-	42	0.15	0.06	0.34	>0
	95	0.25	0.11	0.16	>0
	153	0.30	0.13	0.53	>0
	212	0.33	0.14	0.80	>0
	272	0.34	0.14	0.57	>0
	331	0.35	0.14	0.72	>0

In discussions, Eq. (4) with $K=1$ describes the experimental data (Fig. 3). This does not mean that we neglect any pQCD contribution at p_{T} as high as 5 GeV/c. The traditional pQCD contributions at high p_{T} are partly included in the first term of Eq. (4). In fact, the first term describes the particles in a p_{T} regime which covers "hydrodynamically-inspired" ansätze at low p_{T} and a part of pQCD-calculated distribution at high p_{T}; and the second term describes the particles in a wider p_{T} regime in which the pQCD has much more contributions.

In the Rayleigh-like distribution we have different distribution widths for different momentum components. Generally speaking, we choose $\sigma_x \geqslant \sigma_y$. In the case of extracting temperature information from the (transverse) momentum distribution, we may use σ_y. The identification of elliptic flow is mainly given by the ratio of σ_x/σ_y. Our results render a positive (in-plane) elliptic flow ($\sigma_x > \sigma_y$) in most cases. In a few cases, there is no elliptic flow ($\sigma_x = \sigma_y$). As examples, the detailed identifications of elliptic flows for Figs. 5–10 are given in Table 3.

According to the definitions of $v_2 = \langle\cos(2\varphi)\rangle$ and $\varphi = \arctan(p_y/p_x)$, as well as Eq. (5), we know that v_2 is a complex function of σ_x and σ_y. We would like to regard this function as an alternative description of v_2. Although the function expression is complex, the calculation process of v_2 is easy using the Monte Carlo method. In a further work [31], Liu et al. reported a detailed investigation on v_2 in terms of σ_x/σ_y and σ_y. The calculated results are in agreement with the available STAR [24, 32] and PHENIX [33] experimental data of the dependence of v_2 on p_{T} for identified particles.

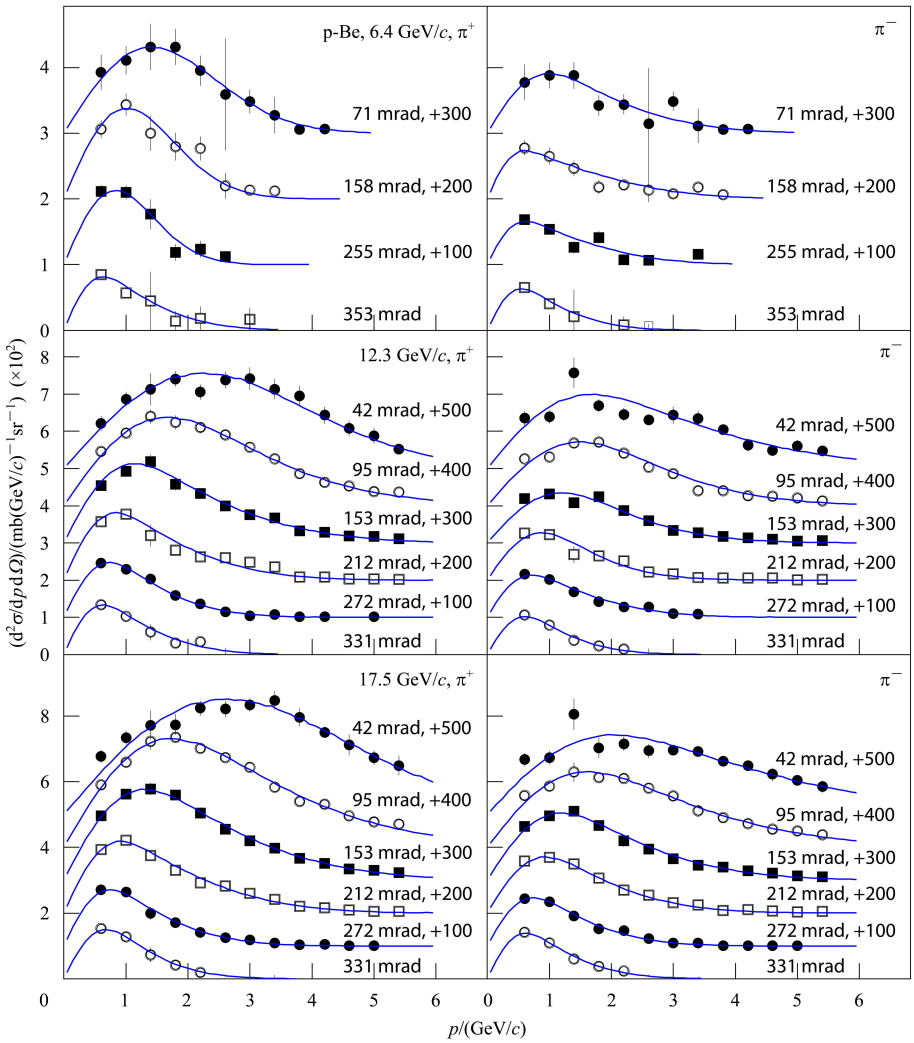

Fig. 5. Momentum distributions of charged pions produced in p-Be collisions at 6.4, 12.3, and 17.5 GeV/c. The circles and squares represent the experimental data of Chemakin et al. [29] for different emission angles. The curves are our results, calculated with Eq. (6).

Although many physically unmotivated models with more than five parameters, e.g. a mixture of power-law and exponential tails, can be chosen in a way as to reproduce the qualitative features of the data, the present work is not a simple physically unmotivated model. In fact, the present work is based on Liu's multisource ideal gas model which describes the angular distribution and correction [22], flow effects [23, 31] and transverse structure of the emission source [34], as well as the multiplicity and multiplicity-like distributions [35, 36]. We choose the Rayleigh-like distribution because it is a natural extension of Liu's multisource ideal gas model. Our modelling result does not mean that a Rayleigh-like tail is better than a power-law spectrum. One can also use the more usual "hydrodynamically-inspired" ansätze at low $p_{\rm T}$, a pQCD-calculated distribution at high $p_{\rm T}$, and coalescence interpolating between the regimes, to describe the $p_{\rm T}$ distributions. The present work provides only a new attempt in the description of $p_{\rm T}$ distributions.

Hydrodynamical ansätze achieve a comparable, if not better, statistical significance at low $p_{\rm T}$ and are well physically motivated. The present work also has a physical significance in the framework of the multisource ideal gas model. The difference between the two models is that the former one focuses its attention on the dynamical characteristics and space-time evolvement of the reaction process and the present work concerns itself with the statistical properties and freeze-out result of the final-state products. It is difficult for us to suggest a way of differentiating experimentally between the two models in the present work.

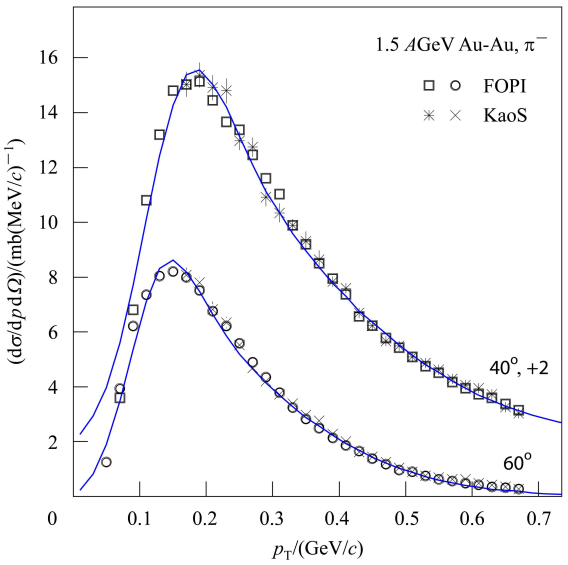

Fig. 6. Momentum distributions of negative pions produced in Au-Au collisions at 1.5 AGeV. The symbols represent the experimental data of the FOPI and KaoS Collaborations [30] for two emission angles. The curves are our results, calculated with Eq. (6).

Finally, we here summarize the physical significance of the present work. The (two-component) Rayleigh-like distribution of transverse momenta is an extension of Liu's multisource ideal gas model. The latter one is an extension of the Maxwell's ideal gas model. The present work gives a new description of $p_{\rm T}$ distributions. From the distribution width σ_y, one can extract source-temperature information. For example, in Au-Au collisions at $\sqrt{s_{\rm NN}}=200$ GeV (Fig. 1), the source temperature extracted from the $p_{\rm T}$ distribution of ϕ particles is 88–217 MeV (from peripheral to central collisions). In Cu-Cu collisions at $\sqrt{s_{\rm NN}}=22.5$ GeV (Fig. 2), the temperature extracted from the $p_{\rm T}$ distribution of $\bar{\rm p}$ is 52–72 MeV. In p-Be collisions at 17.5 GeVc (Fig. 5), the temperature extracted from the momentum distribution of π^- is 26–140 MeV (from small to great ϑ).

The ratio of σ_x to σ_y gives an alternative description of v_2. Specially, $\sigma_x/\sigma_y>1$ describes a positive v_2 flow, and $\sigma_x/\sigma_y=1$ renders that there is no flow [31]. The ratio in peripheral collisions is greater than that in central collisions (Figs. 1 and 2). This means that the v_2 flow in peripheral collisions is large. The ratio also gives a description of the source shape in transverse momentum space. In particular, $\sigma_x/\sigma_y>1$ describes a relative large expansion along the ox axis, and $\sigma_x/\sigma_y=1$ renders an isotropic source in the xoy plane [34]. Our result shows that the source shape in peripheral collisions has a large deformation.

References

1 Bearden I G et al (BRAHMS collaboration). Phys. Rev. Lett., 2002, **88**: 202301
2 Adcox K et al (PHENIX collaboration). Phys. Rev. Lett., 2002, **89**: 092302
3 Abreu M C et al. Phys. Lett. B, 2002, **530**: 33
4 Singh G, Sengupta K, Jain P L. Phys. Rev. Lett., 1988, **61**: 1073
5 Albrecht R et al. Z. Phys. C, 1992, **55**: 539
6 Jain P L, Singh G, Sengupta K. Phys. Rev. C, 1999, **43**: 2027
7 Arsene I et al. Phys. Rev. Lett., 2003, **91**: 072305
8 Ahle L et al (E802 collaboration). Phys. Rev. C, 1999, **59**: 2173
9 Nystrand J I et al. Nucl. Phys. A, 1994, **566**: 419c
10 Bearden I G et al (BRAHMS collaboration). Phys. Rev. Lett., 2004, **93**: 102301
11 Back B B et al (E917 collaboration). Phys. Rev. Lett., 2001, **86**: 1970
12 Bearden I G et al (BRAHMS collaboration). Phys. Lett. B, 2001 **523**: 227
13 Barette J et al (E877 collaboration). Phys. Rev. C, 2000, **62**: 024901
14 Back B B et al (PHOBOS collaboration). Phys. Rev. Lett., 2001, **87**: 102303
15 Bass S A et al. Nucl. Phys. A, 1999, **661**: 205
16 Soff S, Randrup J, Stocker H, XU N. Phys. Lett. B, 2003, **551**: 115
17 Bass S A, Muller B, Srivastava D K. Phys. Rev. Lett., 2003, **91**: 052302
18 TANG Z B et al. Phys. Rev. C, 2009, **79**: 051901(R)
19 Armesto N et al. J. Phys. G, 2008, **35**: 054001
20 LIU F H. Chin. Phys. B, 2008, **17**: 2458
21 LIU F H. Nucl. Phys. A, 2008, **808**: 160
22 LIU F H, Abd Allah N N, Singh B K. Phys. Rev. C, 2004 **69**: 057601
23 LIU F H, LI J S, DUAN M Y. Phys. Rev. C, 2007, **75**: 054613
24 Abelev B I et al (STAR collaboration). Phys. Rev. Lett., 2007, **99**: 112301
25 Mitchell J T for the PHENIX collaboration. arXiv:0701079 [nucl-ex], 2007, Talk given at the 3rd International Workshop on the Critical Point and Onset of Deconfinement, Florence, Italy, July 2006
26 Adare A et al (PHENIX collaboartion). arXiv:0711.3917v1 [nucl-ex], 2007
27 Adler S S et al (PHENIX collaboration). arXiv:0611020 [hep-ex], 2006
28 Bickley A for the PHENIX collaboration. arXiv:0701037v1 [nucl-ex], 2007
29 Chemakin I et al. Phys. Rev. C, 2008, **77**: 015209; and its Erratum, ibid., C, 2008, **77**: 049903(E)
30 Reisdorf W et al (FOPI collaboration). Nucl. Phys. A, 2007, **781**: 459
31 LIU F H, LI J S. Acta Phys. Pol. B, 2008, **40**: 331
32 Adams J et al (STAR collaboration). Phys. Rev. Lett., 2004, **92**: 052302
33 Afanasiev S et al (PHENIX collaboration). Phys. Rev. Lett., 2007, **99**: 052301
34 LIU F H. Chin. Phys. B, 2008, **17**: 883
35 LIU F H. Nucl. Phys. A, 2008, **810**: 159
36 LIU F H, LI J S. Phys. Rev. C, 2008, **78**: 044602